J Mater Sci (2020) 55:14166–14178

Chemical routes to materials

Tailoring structure, morphology and up-conversion properties of CaF_2:Yb^{3+},Er^{3+} nanoparticles by the route of synthesis

Dominika Przybylska[1] and Tomasz Grzyb[1,*]

[1] *Department of Rare Earths, Faculty of Chemistry, Adam Mickiewicz University in Poznań, Uniwersytetu Poznańskiego 8, 61-614 Poznan, Poland*

Received: 19 April 2020
Accepted: 5 July 2020
Published online: 15 July 2020

ABSTRACT

Control of morphology and spectroscopic properties during the synthesis of up-converting nanoparticles (NPs) is a great challenge. One of the most popular ways of NPs synthesis is the hydrothermal method, which is relatively simple, effective, environmentally friendly and permits easy control of synthesis parameters. For these reasons, the hydrothermal method was applied for the synthesis of CaF_2:Yb^{3+},Er^{3+} NPs and optimized. The effects of synthesis conditions on the properties of the product were carefully analysed. The tests were performed to check the impact of two surfactants: sodium citrate (NaCit) and ammonium citrate (NH_4Cit), different excess of ammonium fluoride used as a precipitation agent and different volumes of solution with reactants. The type of co-reagent was found to influence the size of the obtained NPs and charge compensation, required after Yb^{3+} and Er^{3+} doping into Ca^{2+} sites. Depending on the synthesis conditions, the formation of Yb^{3+} clusters and alterations in the Yb^{3+} site symmetry were detected. The excitation and emission spectra revealed the importance of the presence of the Na^+ ions on the energy transfer mechanism and the resulting emission intensity. The presented results show that applying stirring during the synthesis or changing the type of anti-agglomeration agent has a great influence on the luminescence intensity and colour as well as maximum of excitation when Yb^{3+} ions are used. Analysis of the excitation spectra and Yb^{3+} emission decays showed the complex structure of CaF_2:Yb^{3+},Er^{3+} NPs, with Yb^{3+} ions in two different environments within the volume of NPs with different site symmetries. The samples prepared in the presence of Na^+ ions were characterized by long Yb^{3+} emission rise times, revealing energy migration between Yb^{3+} at different symmetries and, at the same time, improved the overall luminescence intensity of NPs.

Address correspondence to E-mail: tgrzyb@amu.edu.pl

https://doi.org/10.1007/s10853-020-05049-9

Introduction

Up-converting nanoparticles (UCNPs) have been intensively investigated in last years because of their unusual properties allowing, in general, for conversion of near-infrared light (NIR) to higher energetic, visible and even ultraviolet [1–5]. This phenomenon can be observed for materials containing lanthanide ions (Ln^{3+}) because of the possibility of electronic transitions within their 4f subshell. Because of the properties of the 4f shell, sharp emission spectra, long luminescence lifetimes and massive Stokes shifts can be observed [6–8]. Nanomaterials containing Ln^{3+} ions are very attractive in many fields of science and industry. Their small size and the possibility of conversion of NIR light make them excellent for many applications, e.g. optical materials, displays, sensors, biological markers, drug delivery systems and many others [9–12].

Considering UCNPs for different applications, particularly in the biomedical field, the ability to control their morphology and spectroscopic properties is essential. These issues are still a challenge [13]. The simplest solution is to adjust the type and conditions of the synthesis route. So far a few main synthesis methods have been proposed, e.g. thermal decomposition, solvo(hydro)thermal synthesis or co-precipitation with polyols [14–16]. The most common and useful method is the thermal decomposition of precursors, which leads to highly uniform nanoparticles of specific shapes and sizes [15, 17–19]. However, in the hydrothermal synthesis, it is also possible to control the conditions so that to obtain particles of desired properties. The hydrothermal synthesis is usually conducted in water, under high pressure and temperature, in a special type of autoclave [15, 20, 21]. Moreover, the process, as well as equipment needed, is quite simple [22–24].

During hydrothermal synthesis, there are many variables like pressure, temperature, synthesis time, the volume of solution or stirring that can significantly influence the morphology and spectroscopic properties of UCNPs. Great importance in synthesis route has also the addition of hydrophilic compounds like sodium citrate, ethylenediaminetetraacetic acid (EDTA), cetyltrimethylammonium bromide (CTAB), as well as polymers, e.g. polyethylene glycol (PEG), polyethylenimine (PEI) and other [14, 16, 25]. These additives not only promote the formation of particles of certain size and shape but also improve the dispersion of UCNPs in water and stabilize the colloids. Additionally, surfactants may affect the spectroscopic properties of NPs.

Calcium fluoride, CaF_2, is one of the best hosts for Ln^{3+} ions, thanks to its stability, low phonon energy, fluorite structure and very good compatibility with Ln^{3+} ions [26–28]. Moreover, CaF_2 is a material with high rigidness, low refractive index and is optically transparent in a range from mid-infrared to UV [29]. As a host compound, CaF_2 can be used in lasers [30], for bioimaging (high biocompatibility with living cell, non-toxic material) [31], biomedical sensors [32] and other applications. Also, this material can be easily obtained by a variety of methods such as sol–gel, solvo(hydro)thermal methods, polyol-mediated, thermal decomposition of precursors or colloidal techniques [33–37]. CaF_2 is also easier to obtain by hydrothermal method as nanocrystals than $NaREF_4$ materials [38–40]. Furthermore, our previous research indicated that using similar to presented here, hydrothermal method, sub-microspheres can be synthesized instead of nanoparticles and by incorporation of Mn^{2+} ions into CaF_2 sub-microspheres the colour of up-conversion can be tuned [41].

In this work, CaF_2 was used as a model, allowing to track the way in which dopant ions are incorporated, which allows for a better understanding of the UC process in similar materials. Moreover, the presented results of synthesis in different volumes or with, and without stirring give insight into problems of production of Ln^{3+}-doped nanomaterials at larger scale.

Experimental section

Characterization

Powder diffractograms were recorded on a Bruker AXS D8 Advance diffractometer, with Cu $K_{\alpha 1}$ radiation $\lambda = 1.5406$ Å. The reference data were taken from the International Centre for Diffraction Data (ICDD). The composition of prepared materials was analysed by energy-dispersive X-ray spectroscopy (EDS), using Quanta 250 FEG, FEI, with voltage 30 kV. Transmission electron microscopy (TEM) images were recorded on a JEOL 1400 Transmission Electron Microscope, which used an accelerating voltage of 120 kV. Fourier transform infrared spectra (FT-IR) were recorded using a JASCO 4200 FT-IR

spectrophotometer. Dynamic light scattering (DLS) and zeta potential measurements were performed by using a Malvern Zetasizer Nano ZS instrument, where the sample concentration was 0.25 mg/mL.

UV–Vis–NIR absorption spectra of powders were recorded with spectrophotometer JASCO V-770. The excitation and emission spectra of the prepared samples in the form of solid powders were measured on a Photon Technology International QuantaMaster™ 40 spectrofluorometer equipped with an Opolette 355LD UVDM tuneable laser, with a repetition rate of 20 Hz and a Hamamatsu R928 photomultiplier used as a detector. A continuous CNI multiwavelength (808, 975, 1208 and 1532 nm) 2 W CW diode laser was used as the excitation source, coupled to a 200 μm optical fibre and collimator for emission measurements and examination of relations between emission intensity and laser power. Laser beam size and power were measured by Ophir 10A-PPS sensor (CW laser) or by Coherent EnergyMax-USB J-10 MB-HE Energy Sensor (pulsed laser). As a detector, a Digital CCD Camera made by Princeton Instruments PIXIS:256E, equipped with an SP-2156 Imaging Spectrograph was applied, corrected for the instrumental response. Luminescence decay curves were recorded using a 200 MHz Tektronix MDO3022 oscilloscope, coupled to the R928 PMT and the QuantaMaster™ 40 spectrofluorometer. All spectra, i.e. excitation and emission were corrected for the instrumental response and OPO laser energy.

Synthesis of CaF_2:20%Yb^{3+},1%Er^{3+} nanoparticles

In order to obtain 3.5 mmol of CaF_2 doped with 20% of Yb^{3+} and 1% of Er^{3+}, the aqueous solution of chlorides with concentration 1 M or 0.25 M was used. $CaCl_2$ (2.77 mmol) and $YbCl_3$ mixed with $ErCl_3$ (0.7 mmol Yb^{3+} and 0.035 mmol Er^{3+}) were added to 20 mL of 1 M aqueous solution of sodium citrate (NaCit) or 20 mL of 1 M aqueous solution of ammonium citrate (NH_4Cit). Then, 5 mL of 2.10 M (1.5 excess to the stoichiometric amount, 1.5 × NH_4F) or 5 mL of 4.2 M aqueous solution of NH_4F (3 times excess to the stoichiometric amount, 3 × NH_4F) as a source of fluoride ions was added to the solution containing $CaCl_2$ and $LnCl_3$ salts. The pH of the final solution was 7.5. The as-prepared transparent solution was transferred into 50 mL (35 mL of solution) or 100 mL (75 mL of solution) Teflon-lined vessel and hydrothermally treated for 12 h (200 °C, 15 bar), in an externally heated autoclave. Two different Berghof autoclaves were used: DAB-2 reactor for the smaller volume sample, without a stirrer, and BR-100 for the larger volume sample, with a stirrer. When the reaction was complete, the obtained white precipitate was purified by centrifugation and rinsed several times with water and ethanol. The final product was dried under ambient conditions. Additionally, CaF_2:20%Yb^{3+}, NaCit, 1.5 × NH_4F in 35 mL of solution was prepared to investigate the influence of complexing agent on spectroscopic properties. Dopant concentrations were established based on literature data and earlier research, as well as synthesis conditions [25, 42].

Results and discussion

Structure and morphology

Cubic nanocrystals of CaF_2 doped with lanthanide ions (Ln^{3+}) were obtained by the hydrothermal synthesis in the presence of sodium citrate (NaCit) or ammonium citrate (NH_4Cit) as a complexing agent. The prepared samples showed a single-phase structure with $Fm\bar{3}m$ space group, for both reactor volumes used (Fig. 1).

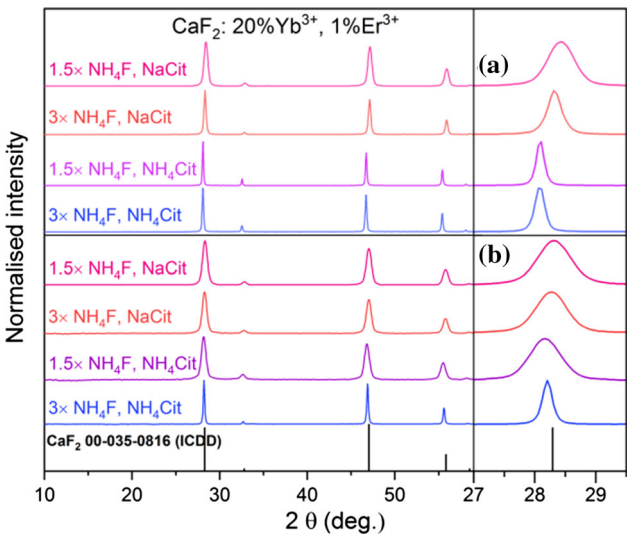

Figure 1 XRD patterns of the CaF_2:Yb^{3+},Er^{3+} samples synthesized by the hydrothermal method: **a** without stirring, in 35 mL volume, **b** with stirring, 75 mL volume. The patterns are labelled according to the scheme: an excess of NH_4F precipitating compound, a source of citric ions.

Additional information about the physical properties of prepared NPs was obtained from the cell parameter analysis (Table S1). An increase in the cell volume of all samples (163.26 to 166.65 Å^3) in comparison with that of undoped CaF_2 (163.04 Å^3) was observed. The larger cell volumes were interpreted as a result of electronic repulsion between F^- ions distributed in a cell in different positions due to local or nonlocal charge compensation as well as clusters formation [43, 44]. Additionally, differences in the cell size between the samples prepared with NaCit and NH_4Cit are presented, which confirms the occurrence of two types of charge compensation processes (1st: 2 $Ca^{2+} \rightarrow Ln^{3+} + Na^+$, 2nd: $Ca^{2+} \rightarrow Ln^{3+} + F^-$). During the synthesis with NaCit, Na^+ ions are incorporated into the structure replacing interstitial fluorine ions because their ionic radii are similar to those of calcium ions (rNa^+ = 1.18, rCa^{2+} = 1.12, for coordination number CN = 8). In the process of synthesis using NH_4Cit, F^- ions act as a charge compensator, as the size of NH_4^+ cations is bigger (rNH_4^+ = 1.54 Å) [45–48]. Moreover, the change of cell size is also noticeable in the XRD patterns (Fig. 1) as a slight shift of the peaks towards lower angles for the samples prepared with NH_4Cit and a shift towards higher angles for the sample with NaCit, obtained in the small volume, with 1.5 × NH_4F excess.

TEM images were used to determine the accurate size of CaF_2 nanoparticles, and the results are listed in Table 1.

NPs sizes were in the range of 17.4–46.5 nm when the small volume was used and 13.8–40.4 nm for the larger volume (Table 1 and Fig. 2). Additionally, some particle agglomerations can be observed in TEM pictures, which was also confirmed by DLS histograms (Fig. S1 in Electronic Supplementary Information, ESI). The tendency to agglomeration is visible mainly for the samples prepared without stirring (Fig. 2a–d). Moreover, the NPs, obtained with the use of NH_4Cit for the synthesis, had irregular shapes and were of larger sizes. To investigate the incorporation of Ln^{3+} ions and the real structure of the obtained compound, EDS mapping was made and the results are presented in Table S2. The amount of Ln^{3+} dopants is lower than assumed, but similar in all samples, i.e. Yb^{3+} 11.03—14.50% and Er^{3+} 0.47—1.14%, with one exception, for the sample prepared in the presence of NH_4Cit with 3 × NH_4F and in 75 mL of solution. The EDS analysis confirmed the incorporation of Na^+ ions into the structure at the sites occupied by Ca^{2+} and F^- ions when the samples were prepared in the presence of NaCit. The amount of Na^+ ions was estimated to be between 16.50 and 28.11%. Additionally, the presence of citrate groups on NPs surface was confirmed by FT-IR measurements (Fig. S2). Prepared samples exhibited negative charge on the surface, except for the samples prepared in the presence of NH_4Cit with 3 × NH_4F in 35 mL, and NH_4Cit, 1.5 × NH_4F in 75 mL (Table S3) which had a positive charge. What is more, the NPs showed different stability in water (zeta potentials varied between |20.3| and |7.8| mV) at physiological pH for 24 h.

Summarizing, it is possible to control the CaF_2:-Yb^{3+},Er^{3+} NPs morphology by selecting the appropriate concentration of NH_4F and the type of co-reagent. From the above-presented results, it is also seen that the synthesis in a reactor with stirring should be more favourable, resulting in lower agglomeration of NPs. It is possible to obtain small NPs of the size below to 20 nm even with a high

Table 1 Size of obtained NPs, calculated from TEM analysis

TEM analysis				
Volume	Stirring	Co-reagent	NH_4F excess	CaF_2:20%Yb^{3+},1%Er^{3+} Size (nm)
35 mL	No	NaCit	1.5 ×	17.4 ± 3.9
			3 ×	27.2 ± 5.8
		NH_4Cit	1.5 ×	35.9 ± 24.7
			3 ×	46.5 ± 11.5
75 mL	Yes	NaCit	1.5 ×	19.5 ± 7.4
			3 ×	14.4 ± 3.4
		NH_4Cit	1.5 ×	13.8 ± 2.4
			3 ×	40.4 ± 11.8

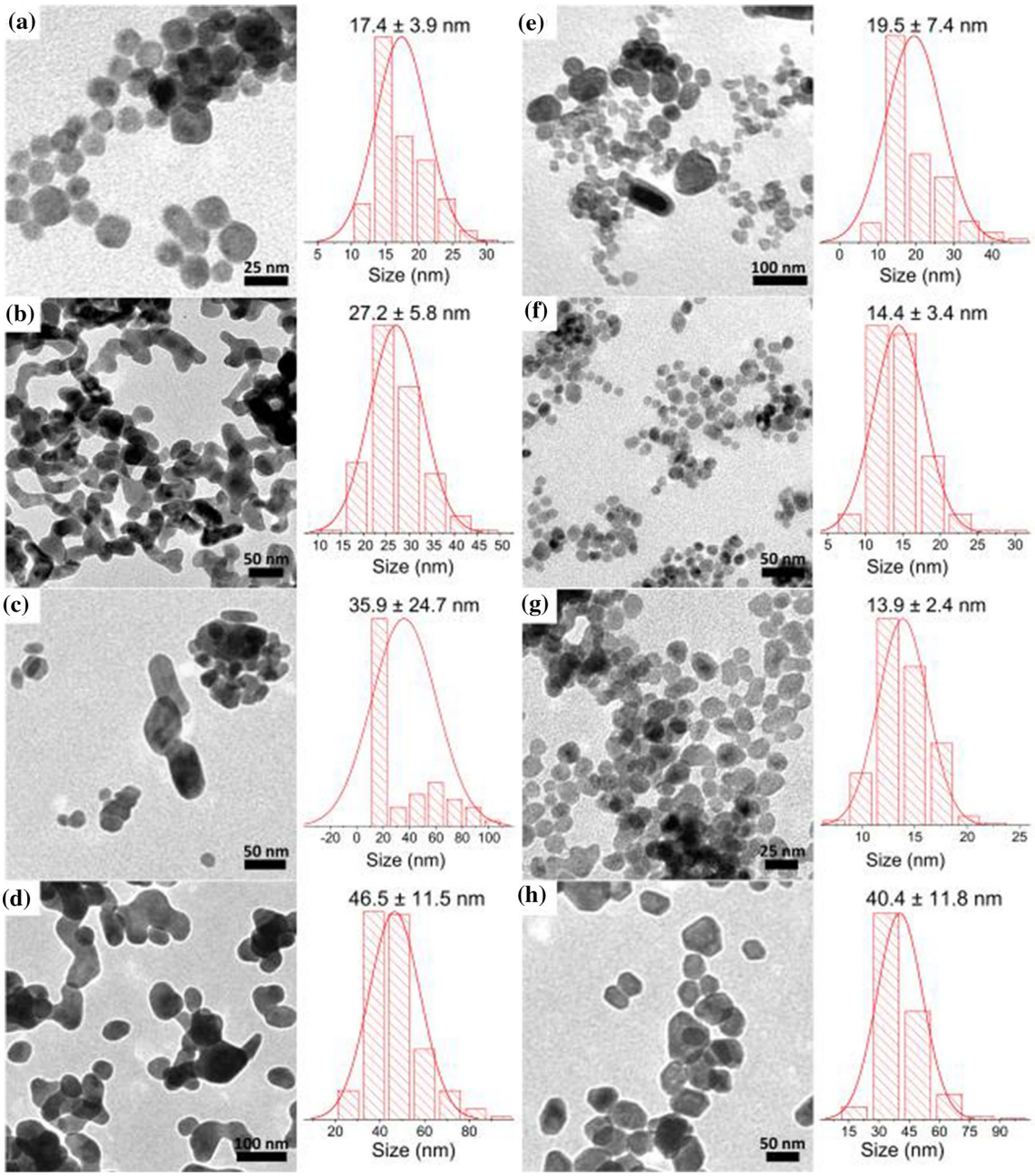

Figure 2 Nanocrystals size distribution of hydrothermally synthesized samples: **a** CaF_2:Yb^{3+},Er^{3+}, NaCit, 1.5 × NH_4F, **b** CaF_2:Yb^{3+},Er^{3+}, NaCit, 3 × NH_4F, **c** CaF_2:Yb^{3+},Er^{3+}, NH_4Cit, 1.5 × NH_4F, **d** CaF_2:Yb^{3+},Er^{3+}, NH_4Cit, 3 × NH_4F, **e** CaF_2:Yb^{3+},Er^{3+}, NaCit, 1.5 × NH_4F, **f** CaF_2:Yb^{3+},Er^{3+}, NaCit, 3 × NH_4F, **g** CaF_2:Yb^{3+},Er^{3+}, NH_4Cit, 1.5 × NH_4F, **h** CaF_2:Yb^{3+},Er^{3+}, NH_4Cit, 3 × NH_4F, where **a**–**d** 35 mL, without stirring, and **e**–**h** 75 mL, with stirring.

content of NH_4F, which is quite essential when the synthesis is conducted in water.

Spectroscopic properties

It is well known from the literature, that only for low concentrations (< 0.1%), the Ln^{3+} dopants form isolated centres. Yb^{3+} ions are sensitive to the site symmetry, and their absorption spectra reflect this feature [49]. The mentioned centres have trigonal,

tetragonal or cubic symmetry, depending on the location of charge compensating F^- ions. In the heavily doped materials, Yb^{3+} ions form clusters, mainly cubooctahedral hexamers with the six Yb^{3+} ions site in square antiprisms [44, 50]. Cluster formation is well confirmed on the basis of the broad Yb^{3+} excitation bands that do not allow drawing conclusions on the Yb^{3+} ions site symmetries as it overlaps any other possible signals. However, for the samples prepared with NaCit, in 35 mL of solution, the formation of centres with the cubic symmetry (O_h) is responsible for the presence of peaks at 966 nm (10,352 cm^{-1}) and 920 nm (10,870 cm^{-1}), which are intense and well separated (Fig. 3a). After Na^+ ions introduction into the structure as a charge compensator, Yb^{3+}–Na^+ ion pairs are formed. At the same time, a decrease in the number of Yb^{3+}–Yb^{3+} pairs and formation of Yb^{2+}, which are responsible for quenching luminescence through cooperative energy transfer from Er^{3+} ions, are observed [47].

As a result, the emission of particles with incorporated Na^+ ions is more intense, which is observed in Figs. 4 and S3. What is interesting, the domination of O_h symmetry is only visible for the sample prepared with NaCit, 3 × NH_4F in 35 mL solution, where more effective incorporation of Na^+ ions replacing interstitial F^- ions occurred. Furthermore, in the analogous sample but prepared in larger volume (75 mL) with stirring, a lower amount of Yb^{3+} sites with the O_h symmetry are present, despite the fact that the determined concentration of Na^+ ions was higher (28%) than for the sample described above. It is worth noting that Na^+ ions can be also present on the surface of NPs due to the bonding to citrate groups, which are incorporated into CaF_2 NPs

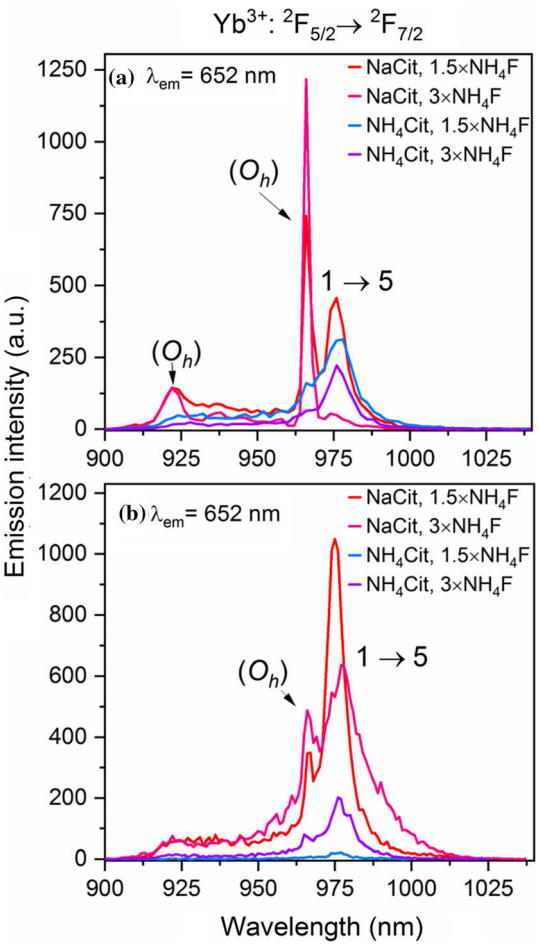

Figure 3 Excitation spectra of CaF_2:20%Yb^{3+},1% Er^{3+} samples (900–1050 nm): **a** small volume, without stirring, **b** large volume, with stirring, excited by pulsed laser as excitation source (at 25 mJ·cm^{-2}).

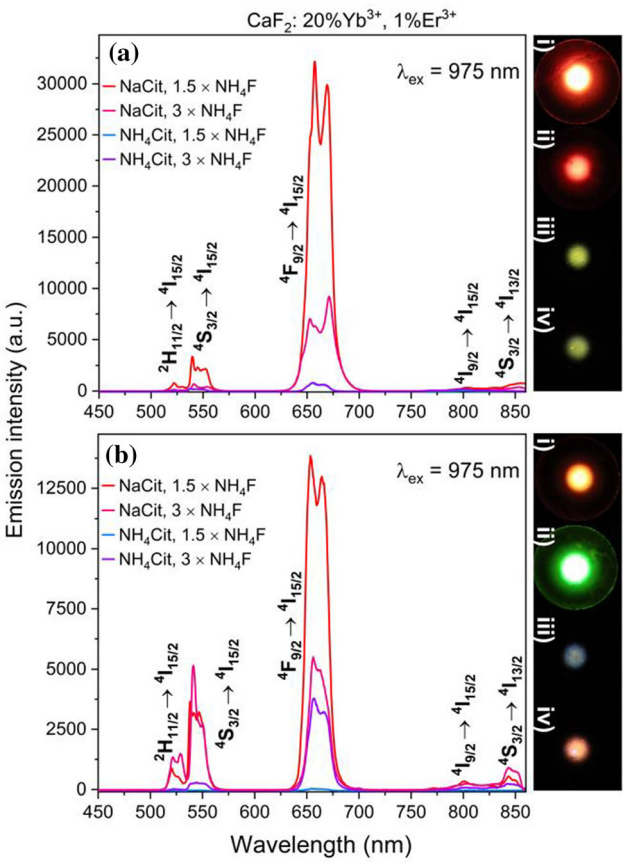

Figure 4 Luminescence (450–860 nm) spectra and emission colour of CaF_2:20%Yb^{3+},1%Er^{3+} samples: **a** small volume, without stirring, **b** large volume, with stirring, where: (i) NaCit, 1.5 × NH_4F, (ii) NaCit, 3 × NH_4F, (iii) NH_4Cit, 1.5 × NH_4F, (iv) NH_4Cit, 3 × NH_4F, excited by laser under continuous excitation source (at 25 W·cm^{-2}).

(Fig. S2). Interestingly, the excitation peak near 966 nm can be detected in the excitation spectra of all of the synthesized samples (Fig. 3), hence confirming the presence of the O_h symmetry of Yb^{3+} ions in the prepared NPs, regardless of the used surfactant, which has been also observed by another research group [44]. Absorption spectra of samples prepared are presented in Fig. S11 showing different characteristics of the Yb^{3+} absorption peaks, hence revealing also different efficiency of energy transfer between various types of Yb^{3+} ions and Er^{3+} ions.

For prepared samples, the emission spectra were measured under continuous diode laser with λ_{ex} = 975 nm wavelength and are presented in Fig. 4. The brightest luminescence was recorded for the samples synthesized in the presence of NaCit and with 1.5 × NH_4F in both volumes used, 35 mL, without stirring and 75 mL with stirring. The observed luminescence intensities confirm the influence of sodium ions on the effectiveness of emission. Additionally, samples prepared without stirring, with NaCit in 35 mL, exhibited twice time stronger emission than the best samples obtained in 75 mL solution with stirring. High luminescence can be connected with a decreased number of formed Yb^{3+}–Yb^{3+} clusters which reduced the non-radiative energy losses. Changes in the cooperative energy transfer between Yb^{3+} ions and shorter distances between Yb^{3+} and Er^{3+} ions (see Table S1) can improve energy transfer.

The synthesis procedure also influences the samples emission colour, which is illustrated in the photographs, the calculated ratios between two of the strongest bands and the chromaticity diagrams (Figs. 4, S4, S5). Interestingly, for the samples prepared without stirring and in the small volume, the domination of red band over green is strongly visible, in comparison with the luminescence of the samples obtained with stirring and in larger volume, for which the $^4S_{3/2} \rightarrow {}^4I_{15/2}$ and $^4F_{9/2} \rightarrow {}^4I_{15/2}$ intensities are similar. As a result, the samples obtained in larger volume, with stirring, showed the yellow-green colour of emission. The most significant shift to the green region was recorded for the sample prepared in 75 mL with stirring, NaCit as co-reagent and 3 × NH_4F, which is also noticeable in Figs. 4b (ii) and S5. Comparing the luminescence of the obtained samples prepared in the same way, it is possible to receive different emission intensity and colour, just by changing the volume and application of stirring.

More information about spectroscopic properties of synthesized CaF_2 NPs was obtained from the luminescence decays of Er^{3+} ions, measured under λ_{ex} = 976 and 966 nm wavelength with pulsed laser as the excitation source (for experimental data, see ESI, Figs. S6 and S7). Moreover, luminescence rise times as well as decays of Yb^{3+} under λ_{ex} = 966/977 nm pulsed laser excitation were also recorded to investigate the energy transfer between Yb^{3+} ions in different sites and the influence of complexing agent on their lifetimes (Fig. S8). On the basis of these measurements, luminescence lifetimes were calculated for transitions of Er^{3+} and Yb^{3+} ions (collected in Tables 2, S4 and S5).

The longest luminescence decay of Er^{3+} ions was recorded for the sample prepared in the presence of NaCit and with 3 × NH_4F, without stirring in 35 mL solution as well as NPs with NaCit, 1.5 × NH_4F, in 75 mL solution. From all Er^{3+} transitions, the decay of $^4F_{9/2} \rightarrow {}^4I_{15/2}$ was recorded as the longest one for all samples (16.4 μs to 206.9 μs), which may be a result of strong emission of this band and the mechanism responsible for $^4F_{9/2}$ energy level excitation. Importantly, for the samples with a large number of Yb^{3+} ions at O_h symmetry sites (NaCit, 1.5 × NH_4F and 3 × NH_4F in 35 mL of solution), longer lifetimes for Er^{3+} were calculated under 966 nm excitation than under 976 nm.

The Yb^{3+} decay time measurements did not reveal significant changes in the lifetimes of Yb^{3+} ions upon excitation with 966 or 976 nm wavelengths, even for the samples with a large number of Yb^{3+} ions at the sites of O_h symmetry. Taking into account a significant impact of site symmetry on Ln^{3+} emission lifetimes, it is expected to find longer lifetimes for the structure with sites of higher symmetry [51]. The explanation of the difference between the literature-based expectation and observations can be the domination of Yb^{3+}–Yb^{3+} clusters in the sample's structure or at least the presence of a mixture of sites of different symmetries, which makes it impossible to excite Yb^{3+} ions at the sites of a single symmetry. However, for the samples prepared in the presence of NaCit, relatively long rise times were observed, especially in comparison with those of the samples obtained with NH_4Cit. What is more, the difference was also detectable for the same samples obtained by the two synthesis routes (NaCit, 3 × NH_4F, 35 mL and NaCit, 3 × NH_4F, 35 mL, Table S5, Fig. 5). The reason for this observation is related to the energy

Table 2 Emission lifetimes calculated from the measured luminescence decay of CaF_2:Yb^{3+},Er^{3+} NPs under 976 nm laser excitation (for decays, see Fig. S6, err < 1.6 μs). The number of photons involved in the up-conversion mechanism, determined from the dependencies of luminescence intensity on laser energy for CaF_2:Yb^{3+},Er^{3+} NPs (for experimental results, see Fig. S9, err < 0.06)

Volume	Stirring	Co-reagent	NH_4F excess	CaF_2:20%Yb^{3+},1%Er^{3+}									
				Lifetime (μs)					Number of photons				
				$^2H_{9/2}$ → $^4I_{15/2}$	$^2H_{11/2}$ → $^4I_{15/2}$	$^4S_{3/2}$ → $^4I_{15/2}$	$^4F_{9/2}$ → $^4I_{15/2}$	$^4I_{9/2}$ → $^4I_{15/2}$	$^2H_{11/2}$ → $^4I_{15/2}$	$^4S_{3/2}$ → $^4I_{15/2}$	$^4F_{9/2}$ → $^4I_{15/2}$	$^4I_{9/2}$ → $^4I_{15/2}$
35 mL	No	NaCit	1.5 ×	22.4	24.2	24.0	99.4	23.9	2.2	2.0	2.0	1.3
			3 ×	39.0	58.4	50.1	200.5	54.2	1.4	1.6	1.6	1.4
		NH_4Cit	1.5 ×	9.5	14.3	14.3	31.3	16.2	1.3	1.4	1.6	1.2
			3 ×	12.1	12.3	12.6	26.7	16.6	1.0	1.1	1.2	1.0
75 mL	Yes	NaCit	1.5 ×	44.1	47.1	49.3	206.9	21.0	1.4	1.3	1.2	1.1
			3 ×	25.3	26.5	24.9	179.8	32.8	1.9	1.7	2.0	1.2
		NH_4Cit	1.5 ×	–	8.4	8.6	16.4	8.2	0.4	0.6	1.2	0.5
			3 ×	–	33.3	33.2	137.5	45.3	1.3	1.4	1.6	1.3

transfer from O_h centres of Yb^{3+} of higher energy (10 352 cm^{-1}) to Yb^{3+} cluster centres with lower energy (10 246 cm^{-1}, 5 → 5 transitions, Fig. 6a). On the basis of these measurements and calculations, it can be concluded that the values of Yb^{3+} lifetimes are independent of the dominant symmetry (the presence or absence of Na^+ ions) as well as of the excitation wavelength. At the same time, the luminescence rise times seem to be sensitive to the site symmetry of Yb^{3+} ions. This result is an additional confirmation of Yb^{3+} ions multisite positions in NPs; there is a fraction at sites of O_h symmetry and a fraction of those in clusters. According to the Hraiech et al., when a high number of Na^+ ions are present in the sample, the band characteristic of Yb^{3+} ions with O_h symmetry appears in the NIR emission spectra with a maximum near 1028 nm. However, when a small number of Na^+ ions were added, or for the samples without sodium ions, only the broad electronic transitions 5 → 3 and 5 → 4 of Stark's level with a band maximum near 1030 and 1050 nm appeared in the spectra [51]. For the all obtained samples, the lifetime, as well as rise time, was measured for the emission at 1050 nm, which proves the presence of Yb^{3+} ions at the sites of O_h symmetry and clusters in all of obtained NPs.

To establish the up-conversion mechanism of the prepared NPs and investigate the effects of the synthesis methodology on it, the dependencies of the luminescence intensity on the laser power were measured. The results of the slope calculations are collected in Table 2 (measurement results, Fig. S9). The slope coefficients calculated for the samples studied took values from the range 1 to 2, which is lower than the theoretical value for energy transitions in Er^{3+} ions [25]. The highest slope coefficient was calculated for the CaF_2: Yb^{3+},Er^{3+} samples prepared with NaCit and 1.5 × NH_4F in the small volume (35 mL), without stirring and with NaCit and 3 × NH_4F with magnetic stirring and in the large volume (75 mL). Such a result can be connected with effective emission, long luminescent lifetimes and high crystallinity of these two samples (appropriate distance between Yb^{3+} and Er^{3+} ions can minimize quenching effects). The highest slope was determined for the $^4F_{9/2}$ → $^4I_{15/2}$ transition. This result can be explained by the relaxation from $^2H_{11/2}$ or $^4S_{3/2}$ level and the highest emission of a band corresponding to the described transition for all samples. For the few prepared nanomaterials, the slope coefficient is close

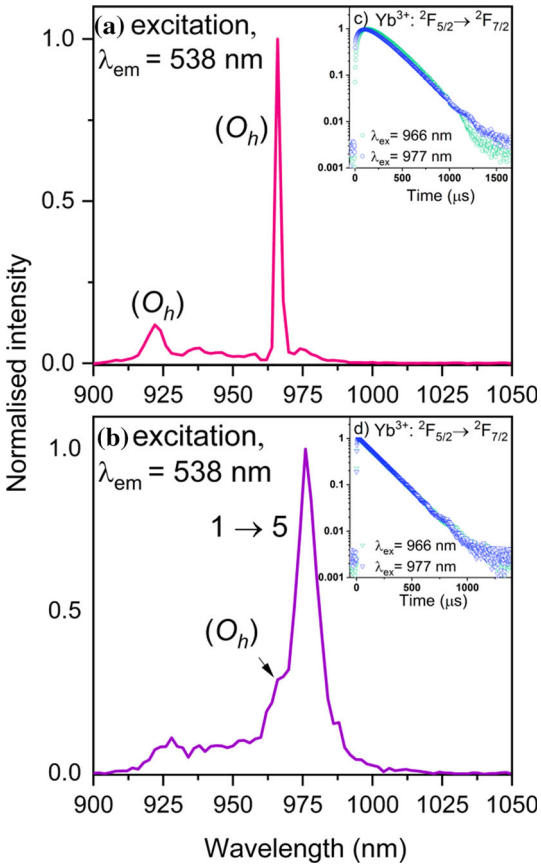

Figure 5 Excitation spectra of CaF_2:Yb^{3+},Er^{3+} **a**, **b** and decay time of Yb^{3+} $^2F_{5/2} \rightarrow {}^2F_{7/2}$ transition **c**, **d** under 966/977 nm pulsed excitation source (at 15 mJ·cm^{-2}), observed at 1050 nm, where **a**, **c** sample with NaCit, 3 × NH_4F, 35 mL solution, **b**, **d** sample with NH_4Cit, 3 × NH_4F, 35 mL solution.

to one; however, the up-conversion emission can be treated as a two-photon process [52]. There are many factors, which can influence the experimental slope like saturation effect, heating of samples or cross-relaxation process between dopants [53, 54]. Furthermore, quite often the saturation effect which is attributed to the competition between linear decay and up-conversion depletion of the intermediate state when excitation density is high takes place [19, 55, 56].

On the basis of the number of photons established for a population of each excited level, a UC mechanism-energy transfer up-conversion (ETU) can be proposed (Figs. 6 and S10). In the first step, Yb^{3+} ion absorbs a photon and excitation of $^2F_{5/2}$ from $^2F_{7/2}$ is observed. For the Yb^{3+} ions at O_h symmetry sites present in the structure, absorption from the ground state to 5, 6 and 7 Stark's sublevel is observed, from which the energy can be transferred to Yb^{3+}–Yb^{3+} clusters or directly to Er^{3+} ions ($^4I_{15/2} \rightarrow {}^4I_{11/2}$ transition). For the hexameric clusters, the energy is absorbed from ground state mostly to 5 Stark's sublevel and transferred to activator ions. These two possible ways of excitation of Yb^{3+} ions can occur simultaneously in one sample with mixed symmetry. The next step of the mechanism is the energy transfer from the excited Yb^{3+}:$^2F_{5/2}$ to Er^{3+}:$^4I_{11/2}$ and the absorption of the second photon, to populate $^4F_{7/2}$, from which relaxation to $^2H_{11/2}$, $^4S_{3/2}$ occurs. Two-photons emission is also observed from $^4F_{9/2}$ and $^4I_{9/2}$ to $^4I_{15/2}$.

Conclusions

Up-converting nanoparticles based on CaF_2 matrix doped with lanthanide ions (Yb^{3+} and Er^{3+}) were synthesized by the hydrothermal method. The

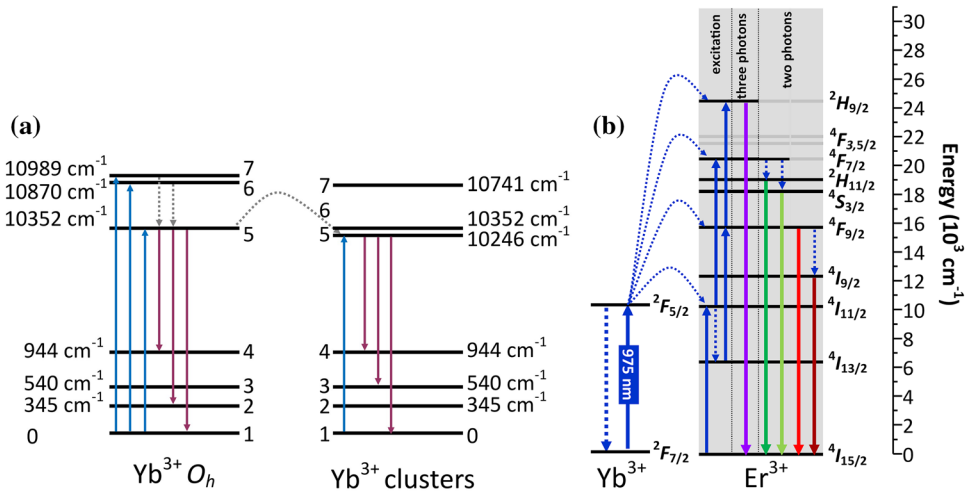

Figure 6 Scheme of the up-conversion mechanism for CaF_2:Yb^{3+},Er^{3+} systems, where **a** proposed mechanism of energy transfer between Yb^{3+} ions with different symmetries, **b** up-conversion energy transfer in Yb^{3+}–Er^{3+} system, under NIR excitation (λ_{ex} = 975 nm).

influence of such factors as the type of co-reagent, excess of fluoride ions, volume and stirring on the morphology and spectroscopic properties of the nanoparticles was investigated. The results provided the evidence illustrating the importance of the synthesis procedure because of its effect on emission intensity, colour and excitation mechanism.

The main factor influencing NPs morphology was the excess of NH_4F; with the higher concentration of F^- ions in the solution, the obtained NPs were bigger. It can be related to a more effective precipitation process. The effect of size of NPs as a result of NH_4F excess used in the synthesis on the spectroscopic properties was also investigated. Moreover, in both synthesis route, the samples prepared with NaCit and 1.5 × NH_4F were characterized by the most intense emission. Additionally, the presence of Na^+ ions changes the symmetry of Yb^{3+} ions, which was visible for the products prepared in 35 mL of the solution without stirring whose luminescence was almost twice higher than that of the other NPs. Moreover, luminescence lifetimes of Er^{3+} and the rise times of Yb^{3+} ions depended on the surfactant used for the synthesis and show that NaCit is more favourable.

Summarizing, we have established the ideal hydrothermal conditions to obtain small NPs with bright up-conversion luminescence under 975 nm (see comparison with $NaYF_4$:Yb^{3+}, Er^{3+} in Fig. S12), which are: synthesis in the presence of NaCit as an anti-agglomeration agent, suppression of NPs growth and 1.5 × NH_4F precipitating agent and 12 h time of synthesis. Avoiding stirring during the reaction and small reaction volume, 35 mL, resulted in the highest intensity of luminescence from all prepared samples. However, increasing reaction volume to 75 mL and the introduction of stirring during synthesis also brought products with satisfactory luminescence intensity and NPs sizes.

Acknowledgements

Funding for this research was provided by the Polish Ministry of Science and Higher Education, Poland, Grant No. ID IP2014014573 and by the National Science Centre, Poland, under Grant No. 2016/22/E/ST5/00016.

Author contributions

DP contributed to conceptualization, investigation, writing—original draft and visualization. TG contributed to conceptualization, resources, writing—review & editing, visualization and supervision.

Compliance with ethical standards

Conflict of interest There are no conflicts to declare.

Electronic supplementary material: The online version of this article (https://doi.org/10.1007/s10853-020-05049-9) contains supplementary material, which is available to authorized users.

References

[1] Li D, Chen G (2019) Upconversion-enhanced dye-sensitized solar cells. In: Dye-sensitized solar cells. Elsevier, pp 325–340

[2] Qin X, Xu J, Wu Y, Liu X (2019) Energy-transfer editing in lanthanide-activated upconversion nanocrystals: a toolbox for emerging applications. ACS Cent Sci 5:29–42. https://doi.org/10.1021/acscentsci.8b00827

[3] Resch-Genger U, Gorris HH (2017) Perspectives and challenges of photon-upconversion nanoparticles—part I: routes to brighter particles and quantitative spectroscopic studies. Anal Bioanal Chem 409:5855–5874. https://doi.org/10.1007/s00216-017-0499-z

[4] Hudry D, Howard IA, Popescu R et al (2019) Structure-property relationships in lanthanide-doped upconverting

nanocrystals: recent advances in understanding core-shell structures. Adv Mater 1900623:1900623. https://doi.org/10.1002/adma.201900623

[5] Auzel F (2004) Upconversion and anti-stokes processes with f and d ions in solids. Chem Rev 104:139–173. https://doi.org/10.1021/cr020357g

[6] Mahalingam V, Thirumalai J, Krishnan R, Mantha S (2016) Up/down conversion luminescence and charge compensation investigation of $Ca_{0.5}Y_{1-x}(WO_4)_2$:xLn^{3+} (Ln = Pr, Sm, Eu, Tb, Dy, Yb/Er) phosphors. Spectrochim Acta A Mol Biomol Spectrosc 152:172–180. https://doi.org/10.1016/j.saa.2015.06.129

[7] Bünzli J-CG, Piguet C (2005) Taking advantage of luminescent lanthanide ions. Chem Soc Rev 34:1048. https://doi.org/10.1039/b406082m

[8] Bünzli JCG (2016) Lanthanide luminescence: from a mystery to rationalization, understanding, and applications. Handb Phys Chem Rare Earths 50:141–176. https://doi.org/10.1016/bs.hpcre.2016.08.003

[9] Niu N, Yang P, Liu Y et al (2011) Controllable synthesis and up-conversion properties of tetragonal $BaYF_5$:Yb/Ln (Ln=Er, Tm, and Ho) nanocrystals. J Colloid Interface Sci 362:389–396. https://doi.org/10.1016/j.jcis.2011.07.001

[10] Sun J, Xian J, Du H (2011) Facile synthesis of well-dispersed SrF_2:Yb^{3+}/Er^{3+} upconversion nanocrystals in oleate complex systems. Appl Surf Sci 257:3592–3595. https://doi.org/10.1016/j.apsusc.2010.11.082

[11] Wang Z-L, Hao J, Chan HLW et al (2011) Simultaneous synthesis and functionalization of water-soluble up-conversion nanoparticles for in-vitro cell and nude mouse imaging. Nanoscale 3:2175. https://doi.org/10.1039/c1nr10090d

[12] Runowski M, Marciniak JJ, Grzyb T et al (2017) Lifetime nanomanometry—high-pressure luminescence of up-converting lanthanide nanocrystals—SrF_2:Yb^{3+}, Er^{3+}. Nanoscale 9:16030–16037. https://doi.org/10.1039/C7NR04353H

[13] Wolfbeis OS (2015) An overview of nanoparticles commonly used in fluorescent bioimaging. Chem Soc Rev 44:4743–4768. https://doi.org/10.1039/C4CS00392F

[14] Escudero A, Becerro AI, Carrillo-Carrión C et al (2017) Rare earth based nanostructured materials: synthesis, functionalization, properties and bioimaging and biosensing applications. Nanophotonics 6:881–921. https://doi.org/10.1515/nanoph-2017-0007

[15] Sun L, Wei R, Feng J, Zhang H (2018) Tailored lanthanide-doped upconversion nanoparticles and their promising bioapplication prospects. Coord Chem Rev 364:10–32. https://doi.org/10.1016/j.ccr.2018.03.007

[16] Yan C, Zhao H, Perepichka DF, Rosei F (2016) Lanthanide ion doped upconverting nanoparticles: synthesis. Struct Prop Small. https://doi.org/10.1002/smll.201601565

[17] DaCosta MV, Doughan S, Han Y, Krull UJ (2014) Lanthanide upconversion nanoparticles and applications in bioassays and bioimaging: a review. Anal Chim Acta 832:1–33. https://doi.org/10.1016/j.aca.2014.04.030

[18] Wang F, Deng R, Liu X (2014) Preparation of core-shell $NaGdF_4$ nanoparticles doped with luminescent lanthanide ions to be used as upconversion-based probes. Nat Protoc 9:1634–1644. https://doi.org/10.1038/nprot.2014.111

[19] Zhou J, Chen G, Zhu Y et al (2015) Intense multiphoton upconversion of Yb^{3+}-Tm^{3+} doped β-$NaYF_4$ individual nanocrystals by saturation excitation. J Mater Chem C 3:364–369. https://doi.org/10.1039/c4tc02363c

[20] Liu Y, Zhang C, Liu H et al (2018) Controllable synthesis of up-conversion nanoparticles UCNPs@MIL-PEG for pH-responsive drug delivery and potential up-conversion luminescence/magnetic resonance dual-mode imaging. J Alloys Compd 749:939–947. https://doi.org/10.1016/j.jallcom.2018.03.355

[21] Shao W, Hua R, Zhang W et al (2013) Hydrothermal synthesis of poly(acrylic acid)-functionalized α-(β-)$NaYF_4$:Yb, Er up-conversion nano-/micro-phosphors. Powder Technol 237:326–332. https://doi.org/10.1016/j.powtec.2012.12.010

[22] Wang M, Abbineni G, Clevenger A et al (2011) Upconversion nanoparticles: synthesis, surface modification and biological applications. Nanomed Nanotechnol Biol Med 7:710–729. https://doi.org/10.1016/j.nano.2011.02.013

[23] Chen J, Zhao JX (2012) Upconversion nanomaterials: Synthesis, mechanism, and applications in sensing. Sensors 12:2414–2435. https://doi.org/10.3390/s120302414

[24] Qiu P, Zhou N, Chen H et al (2013) Recent advances in lanthanide-doped upconversion nanomaterials: synthesis, nanostructures and surface modification. Nanoscale 5:11512. https://doi.org/10.1039/c3nr03642a

[25] Przybylska D, Ekner-Grzyb A, Grześkowiak BF, Grzyb T (2019) Upconverting SrF_2 nanoparticles doped with Yb^{3+}/Ho^{3+}, Yb^{3+}/Er^{3+} and Yb^{3+}/Tm^{3+} ions—optimisation of synthesis method, structural, spectroscopic and cytotoxicity studies. Sci Rep 9:8669. https://doi.org/10.1038/s41598-019-45025-1

[26] Lin M, Zhao Y, Wang S et al (2012) Recent advances in synthesis and surface modification of lanthanide-doped upconversion nanoparticles for biomedical applications. Biotechnol Adv 30:1551–1561. https://doi.org/10.1016/j.biotechadv.2012.04.009

[27] Li Y, Liu T, Du Y (2012) Accelerated fabrication and upconversion luminescence of Yb^{3+}/Er^{3+}-Codoped CaF_2 nanocrystal by microwave heating. Appl Phys Express 5:7–10. https://doi.org/10.1143/APEX.5.086501

[28] Cortelletti P, Pedroni M, Boschi F et al (2018) Luminescence of Eu^{3+} activated CaF_2 and SrF_2 nanoparticles: effect of the

particle size and codoping with alkaline ions. Cryst Growth Des 18:686–694. https://doi.org/10.1021/acs.cgd.7b01050

[29] Ansari AA, Yadav R, Rai SB (2017) Physiochemical properties of greatly enhanced photoluminescence of aqueous dispersible upconversion CaF_2:Yb/Er nanoparticles. Photochem Photobiol Sci 16:890–896. https://doi.org/10.1039/c6pp00448b

[30] Kaczmarek SM, Tsuboi T, Ito M et al (2005) Optical study of Yb^{3+}/Yb^{2+} conversion in CaF_2 crystals. J Phys-Condens Mat 17:3771–3786. https://doi.org/10.1088/0953-8984/17/25/005

[31] Misiak M, Skowicki M, Lipiński T et al (2017) Biofunctionalized upconverting CaF_2:Yb, Tm nanoparticles for Candida albicans detection and imaging. Nano Res 10:3333–3345. https://doi.org/10.1007/s12274-017-1546-y

[32] Marino V, Astegno A, Pedroni M et al (2014) Nanodevice-induced conformational and functional changes in a prototypical calcium sensor protein. Nanoscale 6:412–423. https://doi.org/10.1039/C3NR04978G

[33] Dolcet P, Mambrini A, Pedroni M et al (2015) Room temperature crystallization of highly luminescent lanthanide-doped CaF_2 in nanosized droplets: first example of the synthesis of metal halogenide in miniemulsion with effective doping and size control. RSC Adv 5:16302–16310. https://doi.org/10.1039/C4RA12006J

[34] Hong BC, Kawano K (2008) Syntheses of CaF_2: Eu nanoparticles and the modified reducing TCRA treatment to divalent Eu ion. Opt Mater (Amst) 30:952–956. https://doi.org/10.1016/j.optmat.2007.05.023

[35] Pandurangappa C, Lakshminarasappa BN, Nagabhushana BM (2010) Synthesis and characterization of CaF_2 nanocrystals. J Alloys Compd 489:592–595. https://doi.org/10.1016/j.jallcom.2009.09.118

[36] Claus F, Marcus R, Trampert K (2006) Polyol-mediated synthesis of nanoscale CaF_2 and CaF_2:Ce, Tb. Small 2:1248–1250. https://doi.org/10.1002/smll.200600140

[37] Aubry P, Bensalah A, Gredin P et al (2009) Synthesis and optical characterizations of Yb-doped CaF_2 ceramics. Opt Mater (Amst) 31:750–753. https://doi.org/10.1016/j.optmat.2008.03.022

[38] Jiang T, Qin W, Di W et al (2012) Citric acid-assisted hydrothermal synthesis of α-$NaYF_4$:Yb^{3+}, Tm^{3+} nanocrystals and their enhanced ultraviolet upconversion emissions. CrystEngComm 14:2302. https://doi.org/10.1039/c2ce06311e

[39] Tang H, Xu Y, Cheng X (2020) Growth and enhanced upconversion luminescence intensity of Mg^{2+} and Cr^{3+} co-doped β-$NaYF_4$:Yb^{3+}/Er^{3+} microcrystals. J Solid State Chem. https://doi.org/10.1016/j.jssc.2020.121229

[40] Sagaidachnaya EA, Konyukhova JG, Kazadaeva NI et al (2020) Effect of hydrothermal synthesis conditions on up-conversion luminescence intensity of β-$NaYF_4$:Er^{3+}, Yb^{3+} particles. Quantum Electron 50:109–113. https://doi.org/10.1070/qel17205

[41] Szczeszak A, Grzyb T, Nowaczyk G, Ekner-Grzyb A (2020) Emission colour changes in the CaF_2 sub-microspheres doped with Yb^{3+}, Er^{3+} and Mn^{2+} ions. J Alloys Compd 817:152718. https://doi.org/10.1016/j.jallcom.2019.152718

[42] Zhao X, Yang Z, Yang X et al (2019) Controlling the multicolor upconversion luminescence in CaF_2 nanocrystals doped with Yb^{3+}, Er^{3+} and Nd^{3+} ions under the excitation of a 808 nm laser. Opt Mater Express 9:4578. https://doi.org/10.1364/ome.9.004578

[43] Zhao J, Zhu YJ, Wu J, Chen F (2015) Microwave-assisted solvothermal synthesis and upconversion luminescence of CaF_2:Yb^{3+}/Er^{3+} nanocrystals. J Colloid Interface Sci 440:39–45. https://doi.org/10.1016/j.jcis.2014.10.031

[44] Petit V, Camy P, Doualan JL et al (2008) Spectroscopy of Yb^{3+}:CaF_2: from isolated centers to clusters. Phys Rev B: Condens Matter Mater Phys 78:1–12. https://doi.org/10.1103/PhysRevB.78.085131

[45] Zhang C, Hou Z, Chai R et al (2010) Mesoporous SrF_2 and SrF_2:Ln^{3+} (Ln = Ce, Tb, Yb, Er) hierarchical microspheres: hydrothermal synthesis, growing mechanism, and luminescent properties. J Phys Chem C 114:6928–6936. https://doi.org/10.1021/jp911775z

[46] Pedroni M, Piccinelli F, Passuello T et al (2013) Water (H_2O and D_2O) dispersible NIR-to-NIR upconverting Yb^{3+}/Tm^{3+} doped MF_2 (M = Ca, Sr) colloids: influence of the host crystal. Cryst Growth Des 13:4906–4913. https://doi.org/10.1021/cg401077v

[47] Su L, Xu J, Li H et al (2005) Codoping Na^+ to modulate the spectroscopy and photoluminescence properties of Yb^{3+} in CaF_2 laser crystal. Opt Lett 30:1003. https://doi.org/10.1364/OL.30.001003

[48] Sidey V (2016) On the effective ionic radii for ammonium. Acta Crystallogr Sect B Struct Sci Cryst Eng Mater 72:626–633. https://doi.org/10.1107/S2052520616008064

[49] Kallel T, Hassairi MA, Dammak M et al (2014) Spectra and energy levels of Yb^{3+} ions in CaF_2 transparent ceramics. J Alloys Compd 584:261–268. https://doi.org/10.1016/j.jallcom.2013.09.057

[50] Nicoara I, Stef M (2012) Study of Na^+ ions influence on the charge compensating defects in CaF_2:YbF_3 crystals using dielectric relaxation. Eur Phys J B 85:1–7. https://doi.org/10.1140/epjb/e2012-20914-8

[51] Hraiech S, Jouini A, Jin Kim K et al (2010) Role of monovalent alkali ions in the Yb^{3+} centers of CaF_2 laser

crystals. Radiat Meas 45:323–327. https://doi.org/10.1016/j.radmeas.2009.11.017

[52] Tymiński A, Grzyb T (2017) Are rare earth phosphates suitable as hosts for upconversion luminescence? Studies on nanocrystalline $REPO_4$(RE=Y, La, Gd, Lu) doped with $Yb^{3+}$and Eu^{3+}, Tb^{3+}, Ho^{3+}, Er^{3+}or Tm^{3+} ions. J Lumin 181:411–420. https://doi.org/10.1016/j.jlumin.2016.09.028

[53] Grzyb T, Gruszeczka A, Wiglusz RJ et al (2012) Multifunctionality of $GdPO_4$:Yb^{3+}, Tb^{3+} nanocrystals—luminescence and magnetic behaviour. J Mater Chem 22:22989. https://doi.org/10.1039/c2jm34863b

[54] Wang F, Deng R, Wang J et al (2011) Tuning upconversion through energy migration in core-shell nanoparticles. Nat Mater 10:968–973. https://doi.org/10.1038/nmat3149

[55] Lei Y, Song H, Yang L et al (2005) Upconversion luminescence, intensity saturation effect, and thermal effect in Gd_2O_3:Er^{3+}, Yb^{3+} nanowires. J Chem Phys 123:174710. https://doi.org/10.1063/1.2087487

[56] Vetrone F, Mahalingam V, Capobianco JA (2009) Near-infrared-to-blue upconversion in colloidal $BaYF_5$:Tm^{3+}, Yb^{3+} nanocrystals. Chem Mater 21:1847–1851. https://doi.org/10.1021/cm900313s